Molecular Modeling of the Interactions of Glutamate Carboxypeptidase II with Its Potent NAAG-Based Inhibitors

Suo-Bao Rong,[†,‡] Jiazhong Zhang,[†] Joseph H. Neale,[§] Jarda T. Wroblewski,[∥] Shaomeng Wang,[⊥] and Alan P. Kozikowski*[,†]

Department of Neurology, Department of Pharmacology, and Lombardi Cancer Center, Drug Discovery Program, Georgetown University Medical Center, 3970 Reservoir Road, Washington, DC 20007, and Department of Biology, Georgetown University, Washington, DC 20057

Received December 10, 2001

Glutamate carboxypeptidase II (GCPII, NAALADase, or NAAG peptidase) is a catalytic zinc metallopeptidase. Its extracellular domain hydrolyzes the abundant neuropeptide, *N*-acetyl-L-aspartyl-L-glutamate (NAAG), to produce *N*-acetylaspartate and glutamate following the synaptic release of this transmitter. Thus, GCPII influences the extracellular concentrations of both glutamate and NAAG. NAAG activates group II metabotropic glutamate receptors, and activation of this receptor has been found to protect against anoxia-induced excitotoxic nerve cell death. In contrast, high levels of glutamate can be neurotoxic. Thus, GCPII is a potential therapeutic target for the reduction of excitotoxic levels of glutamate and enhancement of extracellular NAAG. To explore the structural basis of the interaction between GCPII and its inhibitors, we modeled the three-dimensional structure of the GCPII extracellular domain using a homology modeling approach. On the basis of the GCPII model, the structures of GCPII in complex with its potent inhibitors 2-(phosphonomethyl)pentanedioic acid (PMPA) and 4,4′-phosphinicobis(butane-1,3-dicarboxylic acid) (PBDA) were built by a computational docking method. The model of GCPII mainly consists of two $\alpha/\beta/\alpha$ sandwiches, between which two zinc ions are quadrivalently coordinated by the His379-Asp389-Asp455-H_2O and the Asp389-Glu427-His555-H_2O clusters, respectively. The ligand binding pocket is situated between these two sandwiches and is comprised of two subpockets: one is a surface-exposed highly positively charged subpocket; the other is a buried hydrophobic subpocket. The positively charged subpocket can accommodate the pharmacophore groups of inhibitor molecules (PMPA and PBDA) through the coordination of Zn^{2+} with their phosphorus functionality and hydrogen-bonding interactions with Arg536, Arg538, and Ser456 (or Asn521), while the hydrophobic subpocket is engaged in hydrophobic and hydrogen-bonding interactions with the nonpharmacophore groups of PBDA. The predicted binding mode is consistent with the experimental data obtained from site-directed mutagenesis. On the basis of the predicted interaction mode, our structure-based design has led to a series of highly potent GCPII inhibitors.

Introduction

Glutamate carboxypeptidase II (GCPII, also known as *N*-acetylated α-linked acidic dipeptidase, NAALADase, or NAAG peptidase) is widely distributed throughout the central nervous system (CNS).[1,2] GCPII hydrolyzes the abundant neuropeptide *N*-acetyl-L-aspartyl-L-glutamate (NAAG) to produce *N*-acetylaspartate and glutamate both in vitro and in vivo.[3] NAAG is the most abundant and widely distributed peptide transmitter in the mammalian nervous system. This transmitter is codistributed in nerve cells with a spectrum of small amine transmitters, including glutamate.[4] NAAG functions as an agonist at group II metabotropic glutamate receptors (mGluRs)[5] but also interacts with the *N*-methyl-D-aspartate (NMDA) receptor.[6] Thus, GCPII is able to terminate the neurotransmitter activity of NAAG and at the same time to generate glutamate, which subsequently acts at the various glutamate receptor subtypes.[4] Indeed, alterations in GCPII activity and NAAG concentration have been observed in CNS diseases that are associated with abnormalities in glutamatergic neurotransmission.[7]

Recent studies have revealed that inhibition of GCPII provides an alternative pathway to neuroprotection during cerebral ischemia by both increasing NAAG and simultaneously decreasing glutamate levels.[8] An increased NAAG concentration could have neuroprotective effects through both activation of group II mGluRs and blockade of NMDA receptors.[5,9] Decreased glutamate availability is expected to be neuroprotective by limiting toxic glutamate receptor activation.[10] GCPII functions as an upstream regulator of glutamate by acting on its precursor NAAG rather than by inhibiting a single receptor subtype. Thus, GCPII has recently received much attention as a therapeutic target with the aim of suppressing glutamate excitotoxicity that leads to several brain disorders.[8] As another point of interest,

* To whom correspondence should be addressed. (A.P.K.) Tel: 202 687 0686. Fax: 202 687 5065. E-mail: kozikowa@georgetown.edu. (S.W.) Tel: 202 687 2028. Fax: 202 687 4032. E-mail: wangs@georgetown.edu.

† Department of Neurology, Georgetown University Medical Center.

‡ Current address: Locus Discovery, Inc., 4 Valley Square, 512 Township Line Road, Blue Bell, PA 19422.

§ Department of Biology, Georgetown University.

∥ Department of Pharmacology, Georgetown University Medical Cente.

⊥ Lombardi Cancer Center, Georgetown University Medical Center.

10.1021/jm010561g CCC: $22.00
Published on Web 08/17/2002

Chart 1

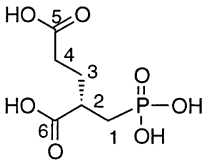

2-(phosphonomethy)pentanedioic acid (PMPA)

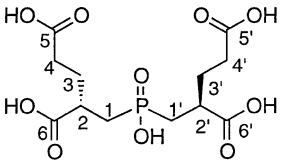

4,4'-phosphinicobis(butane-1,3-dicarboxylic acid) (PBDA)

inhibition of GCPII activity has been found to decrease the perception of chronic pain.[11]

GCPII was first cloned and sequenced as a prostate specific membrane antigen[12] and subsequently cloned as cDNA from human and rat brain tissue.[13] GCPII is a class II membrane glycoprotein that contains a short cytoplasmic amino terminus, a single membrane-spanning domain, and a large extracellular domain. The extracellular domain of GCPII displays sequence similarities to aminopeptidases from *Streptomyces griseus* (SGAP, SWISS-PROT accession number: P80561)[14] and *Vibrio proteolyticus* (AMP, Q01693),[15] which are cocatalytic zinc metallopeptidases belonging to the peptidase family M28.[16] These peptidases have a binuclear zinc binding pocket in which the two zinc ions share a bridging carboxylate ligand. This conservation of the binuclear zinc binding sites was also found in the structure of carboxypeptidase G2 (CPG2, P06621),[17] which hydrolyzes the α-linked glutamate from folic acid. On the basis of the sequence similarity of GCPII to these M28 family members, the specific zinc-coordinating residues in the catalytic site of GCPII were predicted to be Asp379, Asp389, Glu427, Asp455, and His555.[16b,d] Site-directed mutagenesis studies confirmed the importance of these residues to the enzyme's activity.[16c]

Some phosphonate and phosphinate analogues of NAAG, such as 2-(phosphonomethyl)pentanedioic acid (PMPA) (Chart 1) and our previously synthesized NAAG-based mimic [4,4′-phosphinicobis(butane-1,3-dicarboxylic acid), PBDA], were shown to act as neuroprotective agents through inhibition of GCPII.[8c,d,18] While these compounds are highly potent inhibitors of the enzyme, they have only limited ability to penetrate the blood−brain barrier due to their strong hydrophilicity. Although structural modifications were performed for the acidic portions of PMPA to seek more lipophilic compounds, these changes resulted in a more than 1000-fold decrease in inhibitory activity.[8d] Recently, we synthesized nanomolar urea-based GCPII inhibitors. Although the urea moiety is less polar than the phosphonic acid group of PMPA, these urea-based analogues still possess highly hydrophilic properties.[18c] Thus, one of our major goals in designing new GCPII inhibitors was to improve the ability of the compounds to penetrate into the brain without loss of inhibitory activity.

Although sequence analysis and site-directed mutagenesis have been employed to map the zinc-coordinating and the substrate-binding residues, these methods did not provide three-dimensional structural details of the substrate binding pocket[16] nor has this information become accessible by other experimental methods. However, the three-dimensional structure of GCPII is needed to understand the structural basis of the inhibitor−GCPII interactions with the aim of designing inhibitors with improved lipophilicity. We have therefore undertaken molecular modeling studies to generate an understanding of the structural basis of the inhibitor−GCPII interactions, which is the subject of the present paper.

Materials and Methods

Sequence Alignment and Homology Modeling. The sequence of GCPII (P70627) was obtained from the SWISS-PROT protein knowledgebase.[19] It was used as a query sequence to search the NCBI's nonredundant Protein Database using an enhanced BLAST-based search approach.[20] On the basis of the sequence similarity of GCPII, two transferrin receptors, and three aminopeptidases revealed by the BLAST search, the multiple sequence alignment was performed using the Web-based Clustal W.[21] Because the quality of homology modeling is highly dependent on the accuracy of sequence alignment,[22] a further adjustment was performed for the sequence alignment based upon the structure−structure alignment retrieved from the FSSP database for the known structures of the transferrin receptors and aminopeptidases[23] and upon the secondary structure and solvent accessibility information obtained from the consensus prediction[24] and Protein Data Bank summary (PDBsum) database,[25] respectively, for the sequences of GCPII and the template protein.

Interactive modeling of the GCPII extracellular domain was carried out on a Silicon Graphics O2 computer using the Homology module implemented in the program package InsightII (Molecular Simulation, Inc., San Diego, CA). The conserved regions of GCPII were modeled based upon the structures of the template proteins. The side chain rotamer library was used to model amino acid substitutions. Deletions and insertions were built by searching the loop database derived from PDB.[26] Two Zn^{2+} ions extracted from the template protein (1AMP)[37a] were merged into the structural model of GCPII.

The model refinement was carried out in a stepwise manner using a stand-alone version of the CHARMM program[27] (version c27b2) with the all-atom version 22 force field[28] running on a Beowulf cluster with 450 MHz Pentium III CPU processors. The force field parameters that were developed by Karplus's group for zinc binding and tested in the molecular dynamics (MD) simulation of carboxypeptidase A were adopted for the minimization and MD simulation.[29] First, the loops with fixed and freed backbone were minimized, respectively, for 500 steps to relax their conformation. Next, the model was solvated by a 15 Å sphere of TIP3P water molecules[30] centered on two zinc ions and energetically minimized with a fixed backbone using the Adopted-Basis Newton−Raphson (ABNR) method for 2500 steps to remove unfavorable contacts. The model was then minimized for 2500 steps using harmonic constraints with a force constant of 20.0 kcal·mol^{-1}·Å^{-2} on the backbone, followed by another 2500 steps with a force constant of 10.0 kcal·mol^{-1}·Å^{-2} on the α carbons. Finally, the whole model was minimized for 5000 steps or until convergence, defined as an energy gradient ≤0.05 kcal·mol^{-1}·Å^{-1}. The final model of GCPII was checked by the program PROCHECK[31] to verify its folding and stereochemical quality.

Docking and Complex Modeling. The GCPII inhibitor molecules, including (*R*)-PMPA, (*S*)-PMPA, and PBDA, were modeled using the InsightII/Discover molecular modeling package. Computational docking was performed using the automated docking method Autodock.[32] First, the grid maps were calculated using the C, H, O, and P atoms as the probe atoms within a three-dimensional grid (22.5 × 22.5 × 22.5 Å^3) centered on two zinc ions. Then, the three ligands (*R*)-PMPA,

(*S*)-PMPA, and PBDA were docked subsequently into the binding pocket of GCPII. Finally, the complex models were soaked by a 15 Å sphere of water molecules surrounding the small molecules and were optimized by energy minimization for 10 000 steps or until an energy gradient of less than 0.05 kcal·mol^{-1}·Å^{-1} was reached.

MD Simulations and Interaction Analysis. The MD simulations, using the minimized models of the complexes described above as the starting structures, began with a 50 ps heating and a 100 ps equilibration period, followed by a 200 ps or longer production run at 300 K with a step size of 0.001 ps. Trajectories were recorded every 0.5 ps during simulations for analysis. A SHAKE algorithm was used to constrain all bonds to hydrogens.[33] A shifted smoothing function was used for the van der Waals interaction and a switch function for the electrostatic energy, in which the cutoff distance parameters are defined as follows: CTOFNB = 12.0 Å; CTONNB = 8.0 Å.[34] The nonbonded list, including neighboring atoms within a 14.0 Å distance, was updated every 0.5 ps.

Because hydrogen bonds play an important role in ligand binding to aminopeptidases,[37] we analyzed the hydrogen-bonding interactions based upon the trajectories of the MD simulations. For the purpose of this analysis, a hydrogen bond (D−H···A) was defined by a distance between the donor and the acceptor atoms of less than 3.0 Å and an angle θ_{D-H-A} of more than 120°. The hydrogen-bonding energies were calculated to evaluate the stability and the strength of the hydrogen bonds. The hydrophobic contacts were also calculated to examine the hydrophobic interactions.

Results and Discussion

Sequence Alignment and Homology Modeling. The BLAST-based search of NCBI's Protein Database revealed that, as previously identified by sequence analyses,[16b,d] the sequence of the GCPII extracellular domain is similar to those of two transferrin receptors (PDB codes: 1DE4 and 1CX8).[35] The sequence analysis showed that the similar segment of the extracellular domain of GCPII and the transferrin receptors may contain an aminopeptidase fold of carboxypeptidase G2 (1CG2)[36] and of aminopeptidases (1AMP, 1IGB, and 1XJO)[37] that possess the catalytic residues conserved in GCPII but not in the transferrin receptors. Thus, it was necessary to use a hybrid template to model the GCPII extracellular domain.

On the basis of the sequence similarity described above, the multiple sequence alignment was achieved for GCPII, the two transferrin receptors, and the three aminopeptidases using Clustal W,[21] followed by further adjustment in terms of the structure−structure alignment between the known structures of the transferrin receptors and the aminopeptidases,[22] as well as secondary structure and solvent accessibility information for GCPII and the template proteins (Figure 1).

Although the sequence of GCPII in the sequence alignment has 18 insertions and four deletions in comparison to that of the transferrin receptors, only six insertions have more than three amino acid residues. All of these larger insertions with 6−11 amino acid residues are located in the solvent-exposed loops connecting adjacent secondary structure elements. The sequence identity between GCPII and the transferrin receptor (1DE4) is 28%, and the sequence similarity is 46%. Furthermore, the distribution of the predicted secondary structural elements of GCPII is similar to those of the transferrin receptors (Figure 1). The amino acid solvent accessibility of GCPII closely resembles that of the transferrin receptors. Accordingly, the transferrin receptor can be used as the template of the GCPII folding.

In the sequence alignment, the structures of the transferrin receptors (1DE4 and 1CX8) are superimposed with those of the aminopeptidases (1AMP and 1XJO) and carboxypeptidase G2 (1CG2), respectively, with an RMSD value of 2.2 and 2.5 Å for the backbone α-carbon atoms. Most importantly, the putative Zn^{2+}-coordinating residues of GCPII proposed by site-directed mutagenesis[16c] are identical to those of the aminopeptidases revealed in their crystal structures.[37] Consequently, the aminopeptidases can be employed to model the Zn^{2+}-coordinating segments of GCPII.

Structural Model of GCPII. (a) Verification of the GCPII Model. The quality of the structural model of GCPII can be judged by several criteria. A Ramachandran plot[38] (Figure 2) of the GCPII model produced by the program PROCHECK[31] shows that 84 and 13% of nonglycine residues fall within the most favored regions and the additional allowed regions, respectively. Only two residues (Thr723 and Glu750) fall beyond the allowed regions. Because these two residues in disallowed regions are located at the C-terminal, their unreasonable configuration will have no effect on the folding of GCPII and the analysis of ligand−protein interactions. PROCHECK also shows that the GCPII model has acceptable main chain and side chain parameters as well as other stereostructural parameters.

(b) Overall Structure. The model of the extracellular domain of GCPII consists of a large α/*β*/α sandwich, a small α/*β*/α sandwich, and an α nonbundle subdomain (Figure 3a). In the larger α/*β*/α sandwich, four parallel *β*-strands (*β*11, *β*12, *β*13, and *β*15), one antiparallel *β*-strand (*β*14), and a pair of antiparallel *β*-strands (*β*1 and *β*10) form a twisted *β*-sheet that is sandwiched by two clusters of α-helices: one includes three (α6, α7, and α9), and the other includes four α-helices (α1, α5, α8, and α10). In the small α/*β*/α sandwich, the *β*-sheet formed by four parallel *β*-strands (*β*5, *β*6, *β*7, and *β*8) is sandwiched between a pair of α-helices (α2 and α3) and an α-helix (α4). In addition, another antiparallel *β*-sheet comprised of four *β*-strands (*β*2, *β*3, *β*4, and *β*9) is proximate to α-helix 4 and packed against the parallel *β*-sheet. The α nonbundle subdomain formed by five C-terminal α-helices (α11, α12, α13, α14, and α15) is packed against the large α/*β*/α sandwich.

At the interface of the two α/*β*/α sandwiches, there exist two Zn^{2+} ions, which are quadrivalently coordinated by the His379-Asp389-Asp455-H_2O and the Asp389-Glu427-His555-H_2O Zn^{2+}-coordinating clusters, respectively (Figure 3b). It is noted that the water molecule and the residue Asp389 form bridges between two Zn^{2+} ions. Five Zn^{2+}-coordinating residues, His379, Asp389, Glu427, Asp455, and His555, are distributed at the end of *β*11, the end of the *β*11-α5 loop, the middle of the *β*12-α6 loop, the beginning of the *β*13-*β*14 loop, and the middle of the *β*15-α10 loop, respectively. Because all of these secondary structural elements contributing to Zn^{2+} coordination are stemming from the large α/*β*/α sandwich, the Zn^{2+} coordination might play a crucial role in maintaining the folding of the large α/*β*/α sandwich.

Figure 1. Sequence alignment of GCPII (SWISS-PROT: P70627), transferrin receptors (1DE4, 1CX8), aminopeptidases (1AMP, 1XJO), and carboxypeptidase G2 (1CG2). Solvent accessibility (e, solvent-exposed; b, buried) of GCPII and the transferrin receptors are shown above and below the sequence alignment, respectively. Secondary structural elements (*H*, α-helix; *E*, *β*-strand) are displayed at the top and bottom of the sequence alignment, respectively, for GCPII and the transferrin receptors. The Zn^{2+}-coordinating residues conserved between GCPII and the aminopeptidases are colored in orange with a light blue background.

A pair of antiparallel *β*-strands (*β*1 and *β*10) are the longest *β*-strands and extend from the large α/*β*/α sandwich to the small α/*β*/α sandwich (Figure 3a). Additionally, hydrogen-bonding interactions occur between the two α/*β*/α sandwiches. On the *β*7-*β*8 loop of the small α/*β*/α sandwich, eight residues form 10 hydrogen bonds with the large α/*β*/α sandwich. On the *β*3-*β*4 loop of the small α/*β*/α sandwich, one residue forms one hydrogen bond with the large α/*β*/α sandwich (Table 1).

(c) Electrostatic Potential Surface and Binding Pocket. The calculation of surface electrostatic potential reveals that one positively charged pocket is formed between two α/*β*/α sandwiches (Figures 3a and 4). This pocket consists of two subpockets: a surface-exposed subpocket (Figure 4a) and a buried subpocket (Figure 4b). The surface-exposed subpocket is highly positively charged since two Zn^{2+} ions as well as several positively charged residues are distributed at the bottom and the wall of this subpocket, respectively (Figure 4a). In contrast, the wall of the buried subpocket is mainly hydrophobic since a number of hydrophobic residues are widely distributed on the wall, whereas the bottom of the subpocket is positively charged at a local area due to the location of two positively charged residues (Arg212, Lys215) in the interior (Figure 4b).

Models of the Inhibitor−GCPII Complexes. (a) PMPA−GCPII Complex. In the model of the complex between GCPII and PMPA, the ligand is accommodated in a "key-lock" style within the highly positively charged subpocket surrounded by the beginning and end segments of the *β*11-α5 loop, the *β*12-α6 loop, the *β*13-*β*14

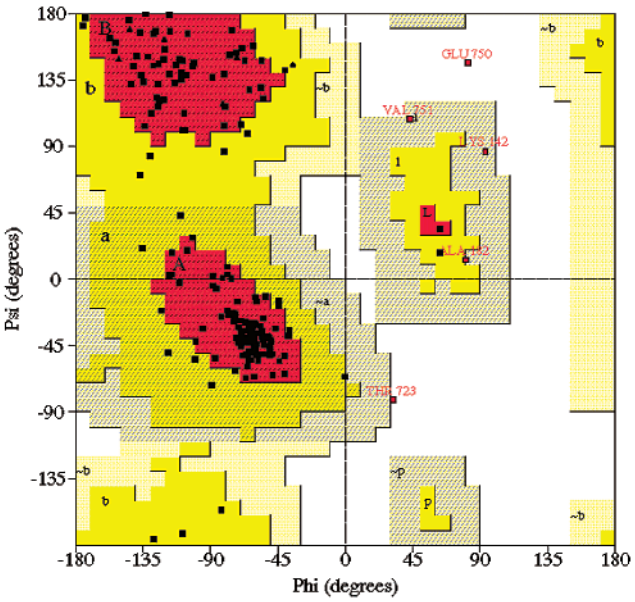

Figure 2. Ramachandran plot for the structural model of GCPII. Glycine residues are shown as triangles; all others as are shown squares. Most favored regions (red), additional allowed regions (yellow), and generously allowed regions (grey yellow) are labeled with capital letters (A, B, L), lower case letters (a, b, l), and a tilde (~a, ~b, ~l, ~p), respectively.

loop, the end of the α8-α9 loop, the strand *β*15, and the *β*15-α10 loop (Figure 5a). In the highly positively charged subpocket, both (*R*)-PMPA and (*S*)-PMPA molecules bind to GCPII in an extended conformation. The structure−activity relationships (SAR) of the propionic acid side chain [$-(CH_2)_2CO_2H$] of PMPA showed that shortening of the side chain by one CH_2 group resulted in a greater decrease of inhibitory activity than lengthening it to $-(CH_2)_3CO_2H$, thus indirectly proving that this side chain may adopt the extended rather than folded conformation to bind to GCPII.[8d]

In the models of the complexes of GCPII with (*R*)-PMPA and (*S*)-PMPA, binding results mainly form two kinds of interactions: one is the Zn^{2+}−phosphonate coordination, and the other is the hydrogen-bonding interaction between the carboxylate groups and the hydrogen bond-forming residues (Figure 5b,c). Within both the (*R*)-PMPA−GCPII and the (*S*)-PMPA−GCPII complex models, the phosphonate group replaces the water molecule that is found bridging the two zinc ions in the model of the free GCPII and bivalently coordinates with those ions. For the (*R*)-PMPA−GCPII complex, the 5- and 6-carboxylate groups interact with the residues Ser456, Arg536, and Arg538 through eight hydrogen bonds, whereas the 5- and 6-carboxylate groups of (*S*)-PMPA form six hydrogen bonds with these three residues.

Because PMPA binds to GCPII principally through Zn^{2+}−phosphonate coordination and hydrogen bonding, the residues that contribute to these two kinds of interactions play determinant roles for GCPII activity. This is supported by the GCPII activity-abolishing mutations of Zn^{2+}-coordinating residues (His379Gly/Ala/Gln, Asp389Glu, Glu427Gln/Asp, Asp455Asn/Leu, and His555Gly/Ala/Gln) and the hydrogen bond-forming residues (Arg538Glu).[16c]

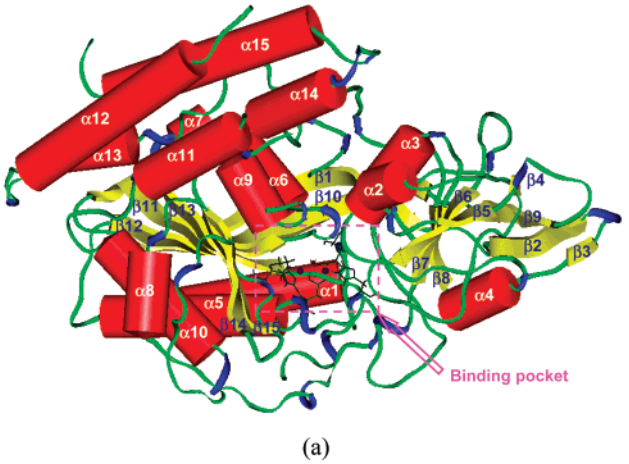

(a)

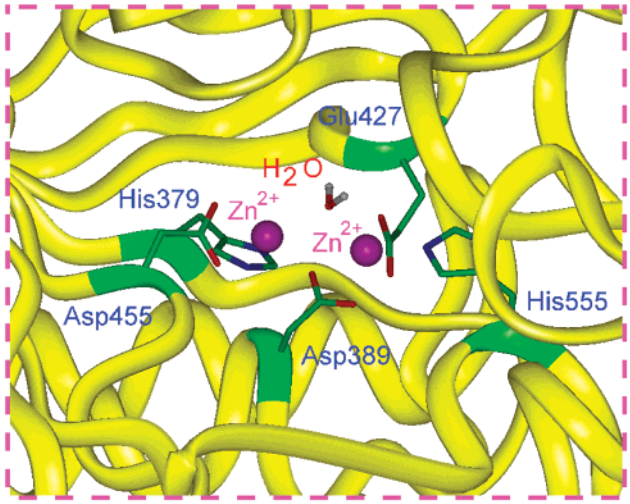

(b)

Figure 3. Structural model of the GCPII extracellular domain. (a) Schematic drawing of the model. The *β*-strands, α-helix, turn, and coils are shown as yellow arrows, red cylinders, blue ribbons, and green ribbons, respectively. The ligand binding pocket surrounding the two Zn^{2+} ions is located between two α/*β*/α sandwiches, in which two Zn^{2+} ions and their coordinating residues are displayed as ball-and-stick, respectively. (b) The two Zn^{2+} ions (ball) are coordinated by the His379-Asp389-Asp455-H_2O and the Asp389-Glu427-His555-H_2O Zn^{2+}-coordinating clusters (stick), respectively.

(b) PBDA−GCPII Complex. Although PBDA is a symmetric molecule, its interaction with GCPII is, of course, not symmetric (Figure 6). In the model of the PBDA−GCPII complex, one portion of the PBDA molecule is located within the surface-exposed highly positively charged subpocket, whereas the other portion is extended into the buried hydrophobic subpocket.

Within the highly positively charged subpocket of GCPII, the PBDA−GCPII interaction mode is similar to that between PMPA and GCPII. The phosphinate group of PBDA bivalently coordinates with two Zn^{2+} ions. The 5- and 6-carboxylate groups of PBDA interact with Asn521, Arg536, and Arg538 of GCPII through five hydrogen bonds. The hydrogen bonds between the Ser456 and the 6-carboxylate group that exist in the PMPA−GCPII complex are not found in the PBDA−GCPII complex, but a new hydrogen bond between the

Table 1. Hydrogen-Bonding Interactions between the Two α/β/α Sandwiches

small α/β/α sandwich		large α/β/α sandwich	
secondary structure	residue	residue	secondary structure
β3-β4 loop	Tyr163 (side chain, HO)[b]	Ser120 (backbone, O)[a]	end of β1
β7-β8 loop	Tyr236 (side chain, HO)[b]	Tyr554 (side chain, OH)[b]	β15-α10 loop
β7-β8 loop	Trp248 (backbone, HN)[b]	His555 (backbone, O)[a]	β15-α10 loop
β7-β8 loop	Trp248 (backbone, O)[a]	His555 (side chain, HN)[b]	β15-α10 loop
β7-β8 loop	Gly267 (backbone, HN)[b]	Gly429 (backbone, O)[a]	β12-α6 loop
β7-β8 loop	Asp268 (side chain, O)[a]	Leu118 (backbone, HN)[b]	end of β1
β7-β8 loop	Asp268 (backbone, HN)[b]	Glu435 (side chain, O1)[a]	middle of α6
β7-β8 loop	Ala276 (backbone, HN)[a]	Glu435 (side chain, O2)[a]	middle of α6
β7-β8 loop	Glu278 (side chain, O)[a]	Arg536 (side chain, HN1)[b]	middle of β10
β7-β8 loop	Glu278 (same as above)[a]	Arg536 (side chain, HN2)[b]	middle of β10
β7-β8 loop	His283 (side chain, HN)[b]	Asp116 (backbone, O)[a]	middle of β1

[a] Acceptor. [b] Donor.

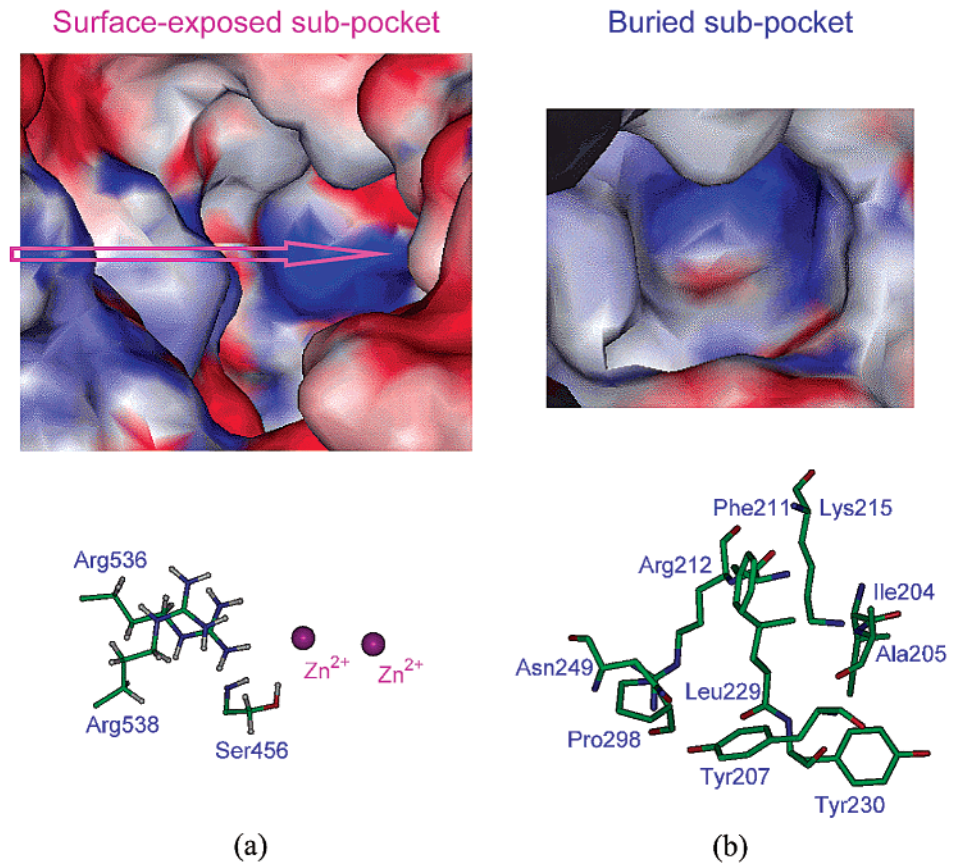

Figure 4. Enlarged ligand binding pocket formed between two α/β/α sandwiches with the same view as in Figure 3. Although only one pocket (a) can be seen at the surface, the binding pocket consists of two subpockets: one is the surface-exposed subpocket, and the other is a buried subpocket. (a) Electrostatic surface of the surface-exposed subpocket. Negative potential is shown in red, and positive potential is shown in blue. This subpocket is highly positively charged due to two Zn^{2+} ions at the bottom and several positively charged residues on the wall. (b) Buried subpocket with the same view as the arrow in panel a. This subpocket is mainly hydrophobic due to the presence of hydrophobic residues that are distributed within this subpocket.

Asn521 and the 5-carboxylate group occurs in the PBDA−GCPII complex (Figures 5 and 6).

Within the buried hydrophobic subpocket, the 5′- and 6′-carboxylate groups of PBDA form hydrogen bonds with Arg212, Asn249, and Leu250, while the hydrophobic chain of PBDA engages in hydrophobic interactions with the remaining part of the buried subpocket.

(c) Pharmacophore Model. Although the ligand−protein interactions are somewhat different in the models of the (*R*)-PMPA−GCPII, (*S*)-PMPA−GCPII, and PBDA−GCPII complexes, similar pharmacophore models have been extracted from these models (Table 2). We have defined the surface-exposed highly positively charged subpocket that interacts with three pharmacophore moieties (two carboxylate groups and one phosphonate/phosphinate group) as the pharmacophore subpocket, whereas the buried hydrophobic subpocket is defined as the nonpharmacophore subpocket.

Analysis of Ligand−GCPII Interactions. As illustrated in Figure 7, the total potential energy and the temperature of all three complex systems remained quite stable during the MD production run, indicating that stable trajectories were obtained in the production run for all three complex models. On the basis of the MD trajectories of the three complex models obtained in the MD production run, the ligand−GCPII interactions were analyzed with regard to three aspects, the

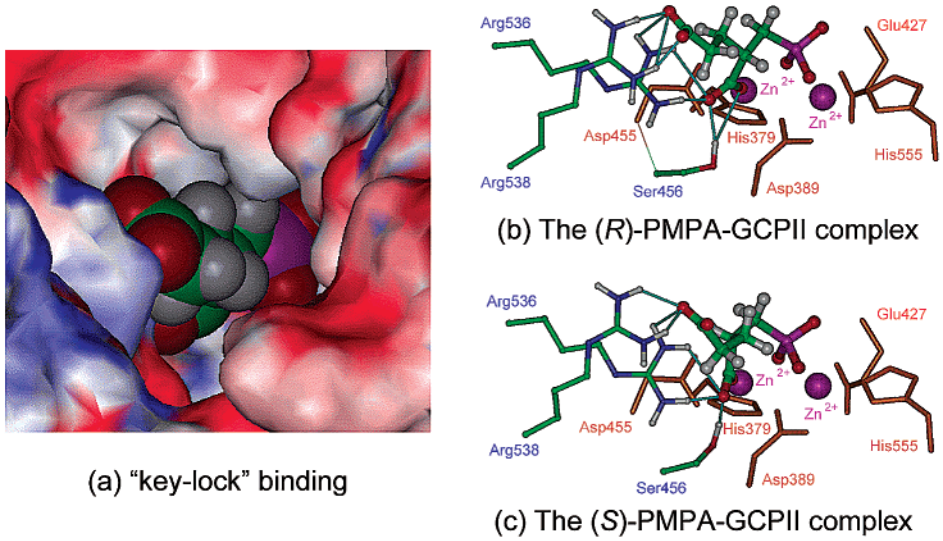

Figure 5. Models of the complexes of GCPII with (*R*)-PMPA and (*S*)-PMPA. (a) The negatively charged (*R*)-PMPA molecule is situated within the highly positively charged subpocket in a "key-lock" style. (b) (*R*)-PMPA binds to GCPII mainly through Zn^{2+} coordination and hydrogen-bonding interactions. (c) (*S*)-PMPA has similar interactions as compared with (*R*)-PMPA. For both (*R*)-PMPA and (*S*)-PMPA, the phosphonate group replaces an original water molecule that bivalently coordinates two Zn^{2+} ions in the uncomplexed GCPII. The 5- and 6-carboxylate groups bind with Arg536, Arg538, and Ser456 through hydrogen-bonding interactions.

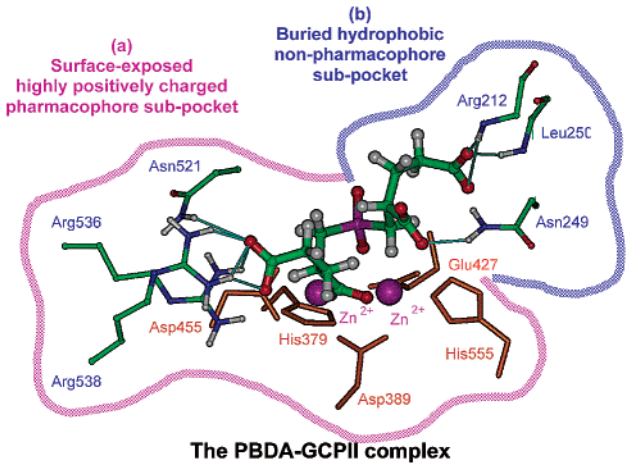

Figure 6. Complex model between GCPII and PBDA. (a) The Zn^{2+}-phosphinate coordination and hydrogen-bonding interactions within the surface-exposed, highly positively charged pharmacophore subpocket. (b) The hydrophobic and hydrogen-bonding interactions within the buried hydrophobic nonpharmacophore subpocket.

Zn^{2+}−phosphonate/phosphinate coordination, hydrogen-bonding interactions, and hydrophobic interactions.

(a) Zn^{2+}−Phosphonate/Phosphinate Coordination. The distances relevant to the Zn^{2+}−phosphonate/phosphinate coordination calculated from the MD trajectories of the models are consistent with those measured for the crystal structures of the aminopeptidases (Table 3).[37] The structural models show that in the inhibitor−GCPII complexes, the two Zn^{2+} ions are quadrivalently coordinated by the His379-Asp389-Asp455-phosphonate/phosphinate and the Asp389-Glu427-His555-phosphonate/phosphinate Zn^{2+}-coordinating clusters, respectively (Figures 5 and 6, Table 3). It is worth noting that when any of the above inhibitor molecules, [(*R*)-PMPA, (*S*)-PMPA, or PBDA] binds to GCPII, the ligand's phosphonate/phosphinate group substitutes an original water molecule of the uncomplexed GCPII and bivalently coordinates with both Zn^{2+} ions. The experimental observation that GCPII activity can be inhibited by ethylenediaminetetraacetic acid (EDTA) and recovered by the addition of $CoCl_2$ reveals that the Zn^{2+} ions play a determinant role for the catalytic function of GCPII.[39] Thus, the Zn^{2+}−phosphonate/phosphinate coordination plays a crucial role in the inhibition of GCPII, which is indirectly confirmed by the already mentioned GCPII activity-abolishing mutations of the Zn^{2+}-coordinating residues.[16c] Furthermore, we have recently observed that the GCPII inhibitory activity of (*S*)-Glu-(*S*)-Glu is 100-fold lower than that of PBDA due to the removal of the Zn^{2+}-coordinating phosphonate group, while the activity of (*S*)-Glu-CO-(*S*)-Glu was only eight times lower because of the presence in this structure of a urea moiety, which is capable of coordinating to Zn^{2+}, albeit more weakly than the phosphonate/phosphinate group.[18c]

(b) Hydrogen-Bonding Interactions. The analysis of hydrogen-bonding interactions (Table 4) showed that several hydrogen bonds are formed between GCPII and the carboxylate groups of (*R*)-PMPA, (*S*)-PMPA, and PBDA. In the model of the complex of GCPII with (*R*)-PMPA, eight hydrogen bonds are formed between three residues (Ser456, Arg536, and Arg538) and the two carboxylate groups of (*R*)-PMPA. Two side chain amino groups of Arg538 form two strong and one weak hydrogen bond, respectively, with two different O atoms of the 5-carboxylate group (Figure 5, Table 4). The weaker hydrogen bond is unstable (Table 4; RMS fluctuation: 1.06). For the residue Arg536, one amino group interacts with the 5- and 6-carboxylate groups through two hydrogen bonds, while the other amino group binds to the 6-carboxylate group through one hydrogen bond. The hydroxyl group of Ser456 forms one strong hydrogen bond and another relatively weak hydrogen bond, respectively, with two different O atoms of the 6-carboxylate group.

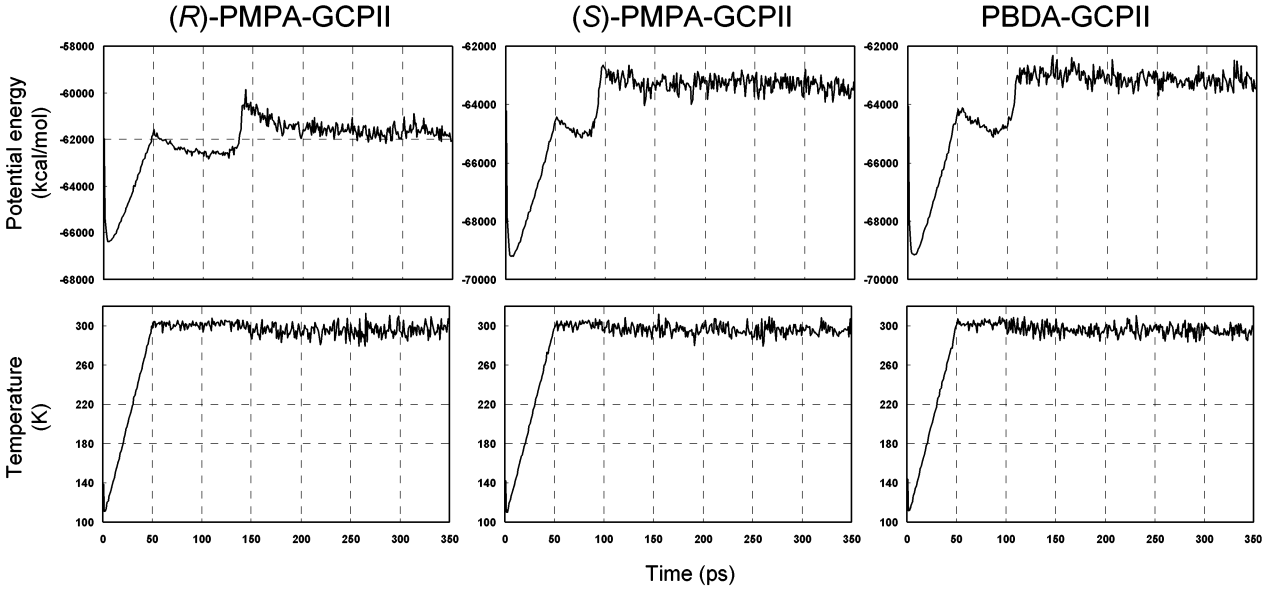

Figure 7. Time evolution of the potential energy and temperature of the complex models of (*R*)-PMPA, (*S*)-PMPA, and PBDA with GCPII.

Table 2. Pharmacophore Models Derived from the Complex Models

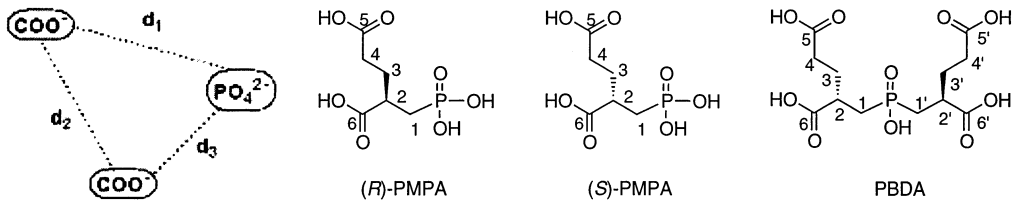

d1 (Å)	7.2	6.8	6.8
d2 (Å)	5.8	5.7	6.2
d3 (Å)	3.6	3.3	3.6

Table 3. Zn^{2+}-GCPII Coordination

		distance (Å)[a]						
Zn^{2+}	$atom_{residue}$	(*R*)-PMPA[b]	(*S*)-PMPA[b]	PBDA[b]	$atom_{residue}$	1AMP[c]	$atom_{residue}$	1XJO[c]
A	$O1_{Asp455}$	2.23 ± 0.04	2.44 ± 0.04	2.48 ± 0.05	$O1_{Asp179}$	2.34	$O1_{Asp160}$	2.62
A	$O2_{Asp455}$	2.10 ± 0.04	2.14 ± 0.03	2.08 ± 0.03	$O2_{Asp179}$	2.05	$O2_{Asp160}$	1.98
A	N_{His379}	2.36 ± 0.04	2.45 ± 0.04	2.44 ± 0.04	N_{His97}	2.21	N_{His85}	2.01
A	$O1_{Asp389}$	2.20 ± 0.03	2.32 ± 0.03	2.11 ± 0.03	$O1_{Asp117}$	2.01	$O1_{Asp97}$	2.08
A	$O1_{phosphonate}$	2.37 ± 0.06	2.18 ± 0.06	2.29 ± 0.11	$O1_{H2O}$	2.29	$O1_{phosphonate}$	2.30
B	$O1_{Glu427}$	2.32 ± 0.06	2.37 ± 0.06	2.44 ± 0.05	$O1_{Glu152}$	2.38	$O1_{Glu132}$	2.67
B	$O2_{Glu427}$	2.02 ± 0.02	2.15 ± 0.03	2.09 ± 0.03	$O2_{Glu152}$	2.04	$O2_{Glu132}$	1.92
B	N_{His555}	2.27 ± 0.03	2.40 ± 0.05	2.23 ± 0.04	N_{His256}	2.32	N_{His247}	1.97
B	$O2_{Asp389}$	1.99 ± 0.02	2.12 ± 0.05	2.11 ± 0.02	$O2_{Asp117}$	2.05	$O2_{Asp97}$	1.99
B	$O2_{phosphonate}$	2.50 ± 0.18	2.35 ± 0.04	2.47 ± 0.06	$O2_{H2O}$	2.25	$O2_{phosphonate}$	1.99

[a] Average value ± RMS fluctuation. [b] Calculated from the MD trajectories. [c] Data taken from the crystal structures of two aminopeptidases (1AMP and 1XJO).

The (*S*)-PMPA−GCPII complex has similar hydrogen-bonding interactions as the (*R*)-PMPA−GCPII complex (Figure 5, Table 4) except that two hydrogen bonds occurring between GCPII and (*R*)-PMPA ($HN1_{Arg538}\cdots O2_{5-C=O}$ and $HO_{Ser456}\cdots O2_{6-C=O}$ in Table 4) are absent in the (*S*)-PMPA−GCPII complex, and one other hydrogen bond ($HO_{Ser456}\cdots O1_{6-C=O}$) is greatly weakened. This difference results from the reversed absolute configuration of the (*S*)-PMPA molecule.

For the PBDA−GCPII complex, two sets of hydrogen-bonding interactions occur within the surface-exposed highly positively charged pharmacophore subpocket and the buried hydrophobic nonpharmacophore subpocket, respectively (Figure 6). In the pharmacophore subpocket, two side chain amino groups of Arg538 form similar hydrogen bonds with the 5-phosphinate group as those found in the (*R*)-PMPA−GCPII complex. The side chain amino group of Arg536 forms only one weak hydrogen bond with the 5-carboxylate group and none with the 6-carboxylate group. Ser456 does not participate in any hydrogen bonds with PBDA. The side chain amide group of Asn521 forms a single hydrogen bond with the 5-carboxylate group of PBDA, which does not occur in the (*R*)-PMPA−GCPII complex. All differences in hydrogen-bonding interactions between the (*R*)-PMPA−GCPII and the PBDA−GCPII complexes result from additional hydrogen bonds between PBDA and GCPII that occur within the nonpharmacophore sub-

Table 4. Hydrogen-Bonding Energies Calculated Based on the MD Trajectories

compd	donor	acceptor	r_{DA} (Å)[a]	θ_{D-H-A} (deg)[a]	θ_{A-H-AA} (deg)[a]	E_{HB} (kcal/mol)[a]
(*R*)-PMPA	$HN1_{Arg538}$	$O1_{5-C=O}$	2.89 ± 0.20	149.1 ± 12.7	119.6 ± 26.3	−3.30 ± 0.22
	$HN1_{Arg538}$	$O2_{5-C=O}$	4.11 ± 0.56	160.5 ± 9.0	58.7 ± 8.2	−1.53 ± 1.06
	$HN2_{Arg538}$	$O1_{5-C=O}$	3.26 ± 0.27	136.4 ± 9.8	138.7 ± 10.6	−3.05 ± 0.40
	$HN12_{Arg536}$	$O1_{5-C=O}$	3.11 ± 0.38	109.6 ± 10.3	115.0 ± 8.5	−3.07 ± 0.47
	$HN11_{Arg536}$	$O1_{6-C=O}$	2.91 ± 0.18	112.0 ± 11.3	122.9 ± 7.1	−3.34 ± 0.19
	$HN2_{Arg536}$	$O1_{6-C=O}$	2.89 ± 0.14	104.1 ± 10.2	117.3 ± 9.5	−3.40 ± 0.13
	HO_{Ser456}	$O1_{6-C=O}$	3.75 ± 0.17	112.5 ± 8.2	75.2 ± 3.5	−2.38 ± 0.32
	HO_{Ser456}	$O2_{6-C=O}$	2.82 ± 0.13	109.4 ± 12.1	123.4 ± 5.6	−4.15 ± 0.14
(*S*)-PMPA	$HN1_{Arg538}$	$O1_{5-C=O}$	2.84 ± 0.12	151.4 ± 11.3	146.6 ± 14.3	−3.40 ± 0.14
	$HN2_{Arg538}$	$O1_{5-C=O}$	3.36 ± 0.29	129.4 ± 7.2	97.9 ± 5.3	−2.91 ± 0.45
	$HN11_{Arg536}$	$O1_{5-C=O}$	3.04 ± 0.21	124.7 ± 6.4	107.4 ± 7.4	−3.30 ± 0.23
	$HN12_{Arg536}$	$O1_{6-C=O}$	3.69 ± 0.38	89.7 ± 7.6	79.7 ± 3.6	−2.35 ± 0.64
	$HN2_{Arg536}$	$O1_{6-C=O}$	3.64 ± 0.21	91.4 ± 7.8	84.2 ± 3.5	−2.46 ± 0.34
	HO_{Ser456}	$O1_{6-C=O}$	4.01 ± 0.18	124.8 ± 3.7	108.6 ± 6.9	−1.89 ± 0.37
PBDA	$HN1_{Arg538}$	$O1_{5-C=O}$	2.75 ± 0.12	130.3 ± 13.1	100.5 ± 11.5	−3.24 ± 0.28
	$HN2_{Arg538}$	$O1_{5-C=O}$	4.38 ± 0.18	106.4 ± 5.7	120.8 ± 7.6	−1.03 ± 0.42
	$HN1_{Arg538}$	$O2_{5-C=O}$	3.16 ± 0.26	102.9 ± 11.7	69.5 ± 9.5	−3.15 ± 0.33
	$HN1_{Arg536}$	$O1_{5-C=O}$	4.02 ± 0.28	108.3 ± 9.3	90.0 ± 6.2	−1.78 ± 0.54
	$HN1_{Asn521}$	$O1_{5-C=O}$	3.85 ± 0.51	112.3 ± 12.3	150.3 ± 8.4	−2.03 ± 0.93
	HO_{Ser456}	$O1_{6-C=O}$	5.42 ± 0.74	99.6 ± 16.4	63.2 ± 5.8	−0.27 ± 0.45
	HN_{Arg212}[b]	$O1_{5'-C=O}$	3.34 ± 0.27	119.7 ± 6.9	86.4 ± 9.2	−2.94 ± 0.46
	HN_{Arg212}[b]	$O2_{5'-C=O}$	3.47 ± 0.25	154.4 ± 7.2	96.8 ± 16.0	−2.73 ± 0.41
	$HN1_{Asn249}$	$O1_{6'-C=O}$	3.21 ± 0.24	125.4 ± 24.3	113.3 ± 17.4	−3.13 ± 0.36
	HN_{Leu250}[b]	$O1_{5'-C=O}$	4.07 ± 0.56	133.4 ± 18.0	133.5 ± 15.5	−1.72 ± 0.92

[a] Average value ± RMS fluctuation. [b] Backbone.

pocket. In this subpocket, four hydrogen bonds are formed between PBDA and GCPII (Figure 6, Table 4). The backbone amide groups of Arg212 and Leu250 interact with the 5′-carboxylate group through two strong and one weak hydrogen bonds, respectively. The side chain amide group of Asn249 forms a single strong hydrogen bond with the 6′-carboxylate group.

It should be noted that the location of the Zn^{2+} ions and hydrogen bond-forming residues within the pharmacophore subpocket imposes strict geometric requirements on potential GCPII inhibitor molecules, i.e., the three pharmacophore moieties of the inhibitor molecule should be complementary with these three binding sites. This requirement is exemplified by our recently synthesized GCPII inhibitors,[18c] of which (*S*)-Asp-CO-(*S*)-Asp has only micromolar activity due to its short side chain situated within the pharmacophore subpocket, whereas (*S*)-Asp-CO-(*S*)-Glu still achieves nanomolar inhibition because the CO-(*S*)-Glu portion of this molecule, like PBDA, remains complementary with the pharmacophore subpocket even though the second amino acid is shortened by one carbon in comparison to PBDA. Additionally, the complementary interaction mode between the three pharmacophore groups and the three binding sites is also consistent with the SAR of PMPA reported by Jackson's laboratory. These authors found that both changing the length of the propionic acid side chain and replacing it with other groups [such as $-CH_2Ph$, $-CH_2CH_2Ph$, $-CH_2$(3-OH−Ph), $-CH_2CH_2$-CN, and $-CH_2CH_2$-tetrazole] led to a more than 500-fold decrease in inhibitory activities.[8d]

(c) Hydrophobic Interactions. The analysis of MD trajectories showed that only one or two hydrophobic contacts occur within the highly positively charged pharmacophore subpocket for the models of the complexes of GCPII with (*R*)-PMPA, (*S*)-PMPA, and PBDA (Table 5). Thus, the inhibitor−GCPII interactions within the pharmacophore subpocket are principally comprised of the Zn^{2+}−phosphonate/phosphinate coordination and hydrogen bonding.

Table 5. Hydrophobic Contacts between GCPII and Ligand

compd	$atom_{lgd}$	$atom_{GCPII}$	distance (Å)[a]
(*R*)-PMPA	C_{3-CH2}	CB_{Asn521}	4.04 ± 0.20
	C_{4-CH2}	$CE2_{Phe211}$	3.92 ± 0.31
(*S*)-PMPA	C_{1-CH2}	CA_{Asn521}	3.98 ± 0.10
PBDA	C_{2-CH2}	CB_{Ser456}	4.18 ± 0.77
	C_{3-CH2}	CB_{Ser456}	3.83 ± 0.57
	$C_{1'-CH2}$	CD_{Glu427}	4.26 ± 0.23
	$C_{3'-CH2}$	CB_{Asn429}	4.26 ± 0.21
	$C_{3'-CH2}$	CG_{Leu250}	4.16 ± 0.14
	$C_{3'-CH2}$	$CD2_{Leu250}$	4.73 ± 0.51
	$C_{4'-CH2}$	CG_{Asn429}	3.83 ± 0.50

[a] Average value ± RMS fluctuation.

In contrast, five hydrophobic contacts were observed within the buried hydrophobic nonpharmacophore subpocket for the model of the PBDA−GCPII complex (Table 5). The 1′-CH_2 group of PBDA undergoes a hydrophobic interaction with the Cδ atom of Glu427. The 3′-CH_2 group participates in hydrophobic interactions with the Cγ and Cδ_2 atoms of Leu250 as well as the Cβ atom of Asn249. The 4′-CH_2 group engages in hydrophobic contacts with the Cγ atom of Asn249. All of these hydrophobic interactions restrict the conformational mobility of PBDA and also play an important role for the binding of PBDA to GCPII.

Interpretation of the SAR within the Nonpharmacophore Subpocket. The inhibitor−GCPII interaction mode revealed by our modeling studies can be used to qualitatively understand the SAR of a series of phosphinic acid analogues recently reported by Jackson's group, which can be written as $HO_2C(HO_2CCH_2CH_2)CHCH_2-PO(OH)-\boldsymbol{R}$. In these compounds, structural changes in the group ***R*** affect the interaction of inhibitors with the nonpharmacophore subpocket while the pharmacophore portion remains fixed.[8d]

The first group of these phosphinic acid analogues are propionic acid derivatives, among which the most potent inhibitor is $HO_2C(HO_2CCH_2CH_2)CHCH_2-PO(OH)-CH_2CH(CH_2CH_2CO_2H)CO_2H$ (IC_{50} = 0.5 nM).[8d] In this compound, replacement of the propionic acid side chain ($CH_2CH_2CO_2H$) by benzyl (CH_2Ph) or methyl (CH_3)

resulted in only a slight (4-fold) decrease in inhibitory activity, whereas the benzyl ester of the methyl analogue [$HO_2C(HO_2CCH_2CH_2)CHCH_2-PO(OH)-CH_2CH(CH_3)CO_2Bn$] had a greatly (190-fold) reduced activity. Although the benzyl and methyl compounds cannot form hydrogen bonds with Arg212 and Leu250, the benzyl and methyl groups, like the two methylene groups of the propionic acid side chain, still contribute to the hydrophobic interactions with the hydrophobic wall of the nonpharmacophore subpocket (Figure 6, Table 5). In contrast, the benzyl ester moiety lacks hydrogen bonding with Asn249 and may severely disturb the hydrophobic interactions within the nonpharmacophore subpocket due to the steric hindrance caused by its benzyl group.

The second group of compounds are the benzyl derivatives. In the parent compound, $HO_2C(HO_2CCH_2CH_2)CHCH_2-PO(OH)-CH_2Ph$, the moiety $-CH_2CH(CH_2CH_2CO_2H)CO_2H$ that binds to the nonpharmacophore subpocket (Figure 6, Table 5) has been replaced by a benzyl group. Although this compound is among the most potent compound in its group, its inhibitory activity ($IC_{50} = 53$ nM) is nevertheless reduced 100-fold relative to $HO_2C(HO_2CCH_2CH_2)CHCH_2-PO(OH)-CH_2CH(CH_2CH_2CO_2H)CO_2H$, as its benzyl group is unable to participate in hydrogen bonding and also might not fit into the nonpharmacophore subpocket due to the planarity of the benzene ring. The introduction of small atoms or groups (such as F, CF_3, and OCH_3) into the benzene ring or the lengthening of benzyl to CH_2CH_2-Ph lead to an insignificant (1−3 times) reduction of activity, while the removal of the benzyl's CH_2 group resulted in a further 60-fold decrease. It is clear from our model (Figure 6) that the direct attachment of the benzene ring to phosphorus greatly interferes with the Zn^{2+}−phosphinate coordination. In contrast, the introduction of small substituents into the phenyl group results in only a slight change of the interactions within the nonpharmacophore subpocket, since this subpocket, due to its relatively larger size, can accommodate these small structural changes.

The third group of compounds are the α-hydroxybenzyl derivatives. In comparison to the parent compound of the second group (***R*** = $-CH_2Ph$), its α-hydroxy derivative [***R*** = −CH(OH)Ph] exhibits approximately the same activity (55 nM), which suggests that the additional hydroxyl group does not significantly modify the interactions within the nonpharmacophore subpocket. However, the introduction of electronegative substituents into the benzene ring [***R*** = −CH(OH)(4-pyridyl) or −CH(OH)−(3-F-Ph)] resulted in an approximately 5-fold increase in inhibitory activity due to a slight enhancement of the electrostatic attraction with the locally positively charged bottom of the nonpharmacophore subpocket.

A fourth group of compounds is represented by the aniline derivative [***R*** = $-CH_2NHPh$]. Although this compound can be regarded as the amine analogue of $HO_2C(HO_2CCH_2CH_2)CHCH_2-PO(OH)-CH_2CH_2Ph$, its activity is 40-fold higher than that of the latter. The key difference between these two substituents is that the former ($-CH_2NHPh$) can form weak hydrogen bonds with the side chains of Glu427 and Asn249, while the latter ($-CH_2CH_2Ph$) does not possess this ability.

GCPII Activity-Abolishing Mutations. Site-directed mutagenesis experiments have revealed that five mutations of the Zn^{2+}-coordinating residues (His379Gly/Ala/Gln, Asp389Glu, Glu427Gln/Asp, Asp455Asn/Leu, and His555Gly/Ala/Gln) and two mutations of the ligand binding residues (Arg538Glu and Lys547Glu) abolish the activity of GCPII.[16c] The Zn^{2+}-coordinating residues are situated at the bottom of the positively charged pocket and coordinate with two Zn^{2+} ions through their negatively charged side chains. The mutations His379-Gly/Ala/Gln, Asp455Asn/Leu, and His555Gly/Ala/Gln may abolish GCPII's ability to coordinate Zn^{2+} due to removal of the Zn^{2+}-coordinating side chains. As for the mutations Asp389Glu and Glu427Asp, although Glu and Asp in principle share their Zn^{2+}-coordinating ability, these mutations could also lead to the loss of Zn^{2+} coordination since side chains of modified length may place the coordinating carboxyl groups in unsuitable locations.

The ligand binding residue Arg538 is located at β-strand 15 and forms strong hydrogen bonds with the carboxylate group of the ligand. Its substitution by a negatively charged Glu (mutation Arg538Glu) completely abolished its ligand binding ability. The residue Lys547 situated at the β15-α10 loop is in proximity to Arg538. When it is mutated to the negatively charged Glu, the local charge distribution is significantly altered, which greatly influences the hydrogen bonding between the Arg538 and the ligand, thus leading to a loss of binding to GCPII.

Except for the above GCPII activity abolishing mutations, four other mutations (Pro390Ala, Glu426Gln, Arg465Ile, and Lys502Arg) have been reported to slightly reduce GCPII activity.[16c] In the model of GCPII, Pro390 is situated at the end of the β11-α5 loop and adjacent to the Zn^{2+}-coordinating residue Asp389. Because Pro390 is a highly constrained residue that is involved in maintaining the conformation of the β11-α5 loop, the mutation Pro390Ala may substantially influence the conformation of the β11-α5 loop so that the orientation of Asp389 is altered, leading to a reduced ability of Asp389 to simultaneously coordinate to both Zn^{2+} ions. The residue Glu426 is located at the β12-α6 loop and forms a hydrogen bond with the Zn^{2+}-coordinating residue Asp379. The mutation Glu426Gln could result in the loss of this hydrogen bond. Consequently, the Zn^{2+}-coordinating residue Asp379 becomes more flexible, thus leading to the reduction of its coordinating ability with Zn^{2+}. As for Arg465, which is located at the middle of β-strand 14, its side chain and backbone form two hydrogen bonds with the backbone of Asn542 and the backbone of Arg538, respectively. When Arg465 is substituted by Ile, its hydrogen bonds with Asn542 will be lost; as a result, the flexibility of residue 465 will be markedly increased. This increased flexibility could weaken the hydrogen bond of residue 465 with the backbone of Arg538, thus leading to enhanced flexibility of Arg538 and consequently to a reduction of its ligand binding ability.

Use of the Structural Models in Structure-Based Design of Novel Inhibitors. On the basis of the above model, we have established a structure-based design strategy for seeking novel or potent GCPII inhibitors. Within the pharmacophore subpocket, we are currently

focusing on the replacement of the phosphonate/phosphinate group by other Zn^{2+}-coordinating groups according to the fixed pharmacophore model illustrated in Table 2, which is consistent with the nanomolar activities observed for our recently synthesized urea-based GCPII inhibitors.[18c] Within the nonpharmacophore subpocket, we are concentrating on the introduction of a hydrophobic group to enhance the hydrophobic interactions with this subpocket. This strategy has led to the synthesis of a series of unsymmetrical urea-based inhibitors, which not only display improved lipophilicity but also retain nanomolar activity. The results will be published in due course.

Summary

The structures of the GCPII extracellular domain and its complexes with the GCPII inhibitors PMPA and PBDA were constructed using homology modeling and computational docking approaches. The GCPII extracellular domain mainly consists of two $\alpha/\beta/\alpha$ sandwiches. One positively charged ligand binding pocket is formed between these two sandwiches. The ligand binding pocket is comprised of two subpockets: one is a surface-exposed highly positively charged pharmacophore subpocket, and the other is a buried hydrophobic nonpharmacophore subpocket. Within the pharmacophore subpocket, the inhibitors (PMPA and PBDA) bind with GCPII through two kinds of interactions: the phosphonate/phosphinate group bivalently coordinates with two Zn^{2+} ions, while the 5- and 6-carboxylate groups interact with the residues Arg536, Arg538, and Ser456 (or Asn521) through hydrogen bonds. Within the nonpharmacophore subpocket, both hydrophobic interactions and hydrogen-bonding interactions occur between GCPII and PBDA. The predicted interaction mode is supported by the site-directed mutagenesis and EDTA inhibition experiments reported in the literature. Furthermore, the derived structure-based design strategy is consistent with the reported activities of our previously synthesized GCPII inhibitors and has led to the design of another series of unsymmetrical GCPII inhibitors with nanomolar potency.

Acknowledgment. This work was supported by the National Institutes of Health (NS 35449, NS 39080, and NS 42672) and Department of Defense (DAMD17-93-V-3018).

References

(1) Blakely, R. D.; Robinson, M. B.; Thompson, R. C.; Coyle, J. T. Hydrolysis of the brain dipeptide *N*-acetyl-L-aspartyl-L-glutamate: subcellular and regional distribution, ontogeny, and the effects of lesions on *N*-acetylated α-linked acidic dipeptidase activity. *J. Neurochem.* **1988**, *50*, 1200−1209. (b) Guarda, A. S.; Robinson, M. B.; Ory-Lavollee, L.; Forloni, G. L.; Blakely, R. D.; Coyle, J. T. Quantitation of *N*-acetyl-aspartylglutamate in microdissected rat brain nuclei and peripheral tissues: findings with a novel liquid-phase radioimmunoassay. *Brain Res.* **1988**, *427*, 223−231. (c) Fuhrman, S.; Palkovits, M.; Cassidy, M.; Neale, J. H. The regional distribution of *N*-acetylaspartylglutamate (NAAG) and peptidase activity against NAAG in the rat nervous system. *J. Neurochem.* **1994**, *62*, 275−281.

(2) Halsted, C. H.; Ling, E.; Luthi-Carter, R.; Villanueva, J. A.; Gardner, J. M.; Coyle, J. T. Folylpoly-γ-glutamate carboxypeptidase from pig jejunum. Molecular characterization and relation to glutamate carboxypeptidase II. *J. Biol. Chem.* **1998**, *273*, 20417−20424.

(3) Robinson, M. B.; Blakely, R. D.; Couto, R.; Coyle, J. T. Hydrolysis of the brain dipeptide *N*-acetyl-L-aspartyl-L-glutamate. Identification and characterization of a novel *N*-acetylated α-linked acidic dipeptidase activity from rat brain. *J. Biol. Chem.* **1987**, *262*, 14498−14506. (b) Stauch, B. L.; Robinson, M. B.; Forloni, G.; Tsai, G.; Coyle, J. T. The effects of *N*-acetylated α-linked acidic dipeptidase (NAALADase) inhibitors on [^{3}H]NAAG catabolism in vivo. *Neurosci. Lett.* **1989**, *100*, 295−300. (c) Stauch-Slusher, B. S.; Tsai, G.; Yoo, G.; Coyle, J. T. Immunocytochemical localization of the *N*-acetyl-aspartyl-glutamate (NAAG) hydrolyzing enzyme *N*-acetylated α-linked acidic dipeptidase (NAALADase). *J. Comput. Neurol.* **1992**, *315*, 217−229. (d) Williamson, L. C.; Eagles, D. A.; Brady, M. J.; Moffett, J. R.; Namboodiri, M. A.; Neale, J. H. Localization and synaptic release of *N*-acetylaspartylglutamate in the chick retina and optic tectum. *Eur. J. Neurosci.* **1991**, *3*, 441−451. (e) Cassidy, M.; Neale, J. H. *N*-acetylaspartylglutamate catabolism is achieved by an enzyme on the cell surface of neurons and glia. *Neuropeptides* **1993**, *24*, 271−278.

(4) Neale, J. H.; Bzdega, T.; Wroblewska, B. *N*-Acetylaspartylglutamate: The most abundant peptide neurotransmitter in the mammalian central nervous system. *J. Neurochem.* **2000**, *75*, 443−452.

(5) Wroblewska, B.; Wroblewski, J. T.; Pshenichkin, S.; Surin, A.; Sullivan, S. E.; Neale, J. H. N-Acetylaspartylglutamate selectively activates mGluR3 receptors in transfected cells. *J. Neurochem.* **1997**, *69*, 174−182. (b) Wroblewska, B.; Santi, M. R.; Neale, J. H. N-Acetylaspartylglutamate activates cyclic-AMP coupled metabotropic glutamate receptors in cerebellar astrocytes. *Glia* **1998**, *24*, 172−180. (c) Wroblewska, B.; Wroblewski, J. T.; Saab, O.; Neale, J. H. N-Acetylaspartylglutamate inhibits forskolin-stimulated cyclic AMP levels via a metabotropic glutamate receptor in cultured cerebellar granule cells. *J. Neurochem.* **1993**, *61*, 943−948. (d) Schaffhauser, H.; Knoflach, F.; Pink, J. R.; Bleuel, Z.; Cartmell, J.; Goepfert, F.; Kemp, J. A.; Richards, J. G.; Adam, G.; Mutel, V. Multiple pathways for regulation of the KCl-induced [^{3}H]-GABA release by metabotropic glutamate receptors, in primary rat cortical cultures. *Brain Res.* **1998**, *782*, 91−104. (e) Cartmell, J.; Adam, G.; Chaboz, S.; Henningsen, R.; Kemp, J. A.; Klingelschmidt, A.; Metzler, V.; Monsma, F.; Schaffhauser, H.; Wichmann, J.; Mutel, V. Characterization of [^{3}H]-(2*S*,2′*R*,3′*R*)-2-(2′,3′-dicarboxycyclopropyl)glycine ([^{3}H]-DCG IV) binding to metabotropic mGluR2 receptor-transfected cell membrane. *Br. J. Pharmacol.* **1998**, *123*, 497−504.

(6) Vallivullah, H. M.; Lancaster, J.; Sweetnam, P. M.; Neale, J. H. High concentrations of N-acetylaspartylglutamate and AMPA, kainate, and NMDA binding sites. *J. Neurochem.* **1994**, *63*, 1714−1719. (b) Sekiguchi, M.; Okamoto, K.; Sakai, Y. Low concentration *N*-acetylaspartylglutamate suppresses the climbing fiber response of Purkinje cells in Guinea pig cerebellar slices and the responses to excitatory amino acids of *Xenopus laevis* oocytes injected with cerebellar mRNA. *Brain Res.* **1989**, *482*, 87−96. (c) Puttfarcken, P. S.; Montgomery, D.; Coyle, J. T.; Werling, L. L. *N*-acetyl-L-aspartyl-L-glutamate (NAAG) modulation of NMDA-stimulated [^{3}H]norepinephrine release from rat hippocampal slices. *Pharmacol. Exp. Ther.* **1993**, *266*, 796−803. (d) Westbrook, G.; Mayer, M. L.; Namboodiri, M. A. A.; Neale, J. H. High concentrations of *N*-acetylaspartylglutamate (NAAG) selectively activate NMDA receptors on mouse spinal cord neurons in cell culture. *J. Neurosci.* **1986**, *6*, 3385−3392. (e) Sekiguchi, M.; Wada, K.; Wenthold, R. J. *N*-acetylaspartylglutamate acts as an agonist upon homomeric NMDA receptor (NMDAR1) expressed in Xenopus oocytes. *FEBS Lett.* **1992**, *311*, 285−289.

(7) Tsai, G.; Passani, L.; Slusher, B.; Carter, R.; Baer, L.; Kleinman, J.; Coyle, J. Abnormal excitatory neurotransmitter metabolism in schizophrenic brains. *Arch. Gen. Psychiatry* **1995**, *52*, 829−836. (b) Rothstein, J. D.; Tsai, G.; Kuncl, R.; Clawson, L.; Cornblath, D. R.; Drachman, D. B.; Pestronk, A.; Stauch-Slusher, B.; Coyle, J. T. Abnormal excitatory amino acid metabolism in amyotrophic lateral sclerosis. *Ann. Neurol.* **1990,** *28*, 18−25. (d) Jaarsma, D.; Veenma-van der Duin, L.; Korf, J. N-Acetylaspartate and *N*-acetylaspartylglutamate levels in Alzheimer's disease post-mortem brain tissue. *J. Neurol. Sci.* **1994**, *127*, 230−233. (e) Passani, L. A.; Vonsattel, J. G.; Carter, R. E.; Coyle, J. T. N-Acetylaspartylglutamate, *N*-acetylaspartate and *N*-acetylated alpha-linked acidic dipeptidase in human brain and their alterations in Huntington's disease and Alzheimer's disease. *Mol. Chem. Neuropathol.* **1997**, *31*, 97−118. (f) Tsai, G.; Slusher, B.; Sim, L.; Hedreen, J. C.; Rothstein, J. D.; Kuncl, R.; Coyle, J. T. Reductions in acidic amino acids and *N*-acetyl-aspartyl-glutamate in amyotrophic lateral sclerosis CNS. *Brain Res.* **1991**, *556*, 151−156. (g) Passani, L. A.; Vonsattel, J. P.; Coyle, J. T. Distribution of *N*-acetylaspartylglutamate immunoreactivity in human brain and its alteration in neurodegenerative disease. *Brain Res.* **1997**, *772*, 9−22. (h) Meyerhoff, J. L.; Koller, K. J.; Walczak, D. D.; Coyle, J. T. Regional brain levels of *N*-acetyl-aspartylglutamate: the effect of kindled seizures. *Brain Res.* **1985**, *46*, 392−396.

(8) Slusher, B. S.; Vornov, J. J.; Thomas, A. G.; Hurn, P. D.; Harukuni, I.; Bhardwaj, A.; Traystman, R. J.; Robinson, M. B.; Britton, P.; Lu, X.-C. M.; Tortella, F. C.; Wozniak, K. M.; Yudkoff, M.; Potter, B. M.; Jackson, P. F. Selective inhibition of NAALADase, which converts NAAG to glutamate, reduces ischemic brain injury. *Nat. Med.* **1999**, *5*, 1396−1402. (b) Thomas, A. G.; Vornov, J. J.; Olkowski, J. L.; Merion, V. T.; Slusher, B. S. N-Acetylated alpha-linked acidic dipeptidase converts *N*-acetylaspartylglutamate from a neuroprotectant to a neurotoxin. *J. Pharmacol. Exp. Ther.* **2000**, *295*, 16−22. (c) Jackson, P. F.; Cole, D. C.; Slusher, B. S.; Stetz, S. L.; Ross, L. E.; Donzati, B. A.; Trainor, D. A. Design, synthesis, and biological activity of a potent inhibitor of neuropeptidase *N*-acetylated-alpha-linked acidic dipeptidase. *J. Med. Chem.* **1996**, *39*, 619−622. (d) Jackson, P. F.; Tays, K. L.; Maclin, K. M.; Ko, Y.-S.; Li, W.; Vitharana, D.; Tsukamoto, T.; Stoermer, D.; Lu, X.-C.; Wozniak, K.; Slusher, B. S. Design and Pharmacological Activity of Phosphinic Acid Based NAALADase Inhibitors. *J. Med. Chem.* **2001**, *44*, 4170−4175.

(9) Bruno, V.; Battaglia, G.; Copani, A.; Giffard, R. G.; Raciti, G.; Raffaele, R.; Shinozaki, H.; Nicoletti, F. Activation of class II or III metabotropic glutamate receptors protects cultured cortical neurons against excitotoxic degeneration. *Eur. J. Neurosci.* **1995**, *7*, 1906−1913. (b) Bruno, V.; Wroblewska, B.; Wroblewski, J. T.; Fiore, L.; Nicoletti, F. Neuroprotective activity of *N*-acetylaspartylglutamate in cultured cortical cells. *Neuroscience* **1998**, *85*, 751−757. (c) Buisson, A.; Choi, D. W. The inhibitory mGluR agonist, *S*-4-carboxy-3-hydroxy-phenylglycine selectively attenuates NMDA neurotoxicity and oxygen-glucose deprivation-induced neuronal death. *Neuropharmacology* **1995**, *34*, 1081−1087.

(10) Rothman, S. M.; Olney, J. W. Glutamate and the pathophysiology of hypoxic-ischemic brain damage. *Ann. Neurol.* **1986**, *19*, 105−111. (b) Meldrum, B. Protection against ischaemic neuronal damage by drugs acting on excitatory neurotransmission. *Cerebrovasc. Brain Metab. Rev.* **1990**, *2*, 27−57.

(11) Carpenter, K. J.; Sen, S.; Dickenson, A. H.; Wozniak, K. M.; Slusher, B. S. Effects of NAALADase inhibition on responses of dorsal horn neurons after inflammation and neuropathy. *Neurosci. Abstr.* **2000**, *30*, 43−49. (b) Yamamoto, T.; Nozaki-Taguchi, N.; Sakashita, Y. Spinal *N*-acetyl-alpha-linked acidic dipeptidase (NAALADase) inhibition attenuates mechanical allodynia induced by paw carrageen injection in the rat. *Brain Res.* **2001**, *909*, 138−144. (c) Yamamoto, T.; Nozaki-Taguchi, N.; Sakashita, Y.; Inagaki, T. Inhibition of spinal *N*-acetylated alpha linked acidic diptptidase produces an antinociceptive effect in the rat formalin test. *Neuroscience* **2001**, *102*, 473−479.

(12) Pinto, J. T.; Suffoletto, B. P.; Berzin, T. M.; Qiao, C. H.; Lin, S. L.; Tong, W. P.; May, F.; Mukherjee, B.; Heston, W. D. W. Prostate-specific membrane antigen: A novel folate hydrolase in human prostatic carcinoma cells. *Clin. Cancer Res.* **1996**, *2*, 1445−1451. (b) Leek, J.; Lench, N.; Maraj, B.; Bailey, A.; Carr, I. M.; Andersen, S.; Cross, J.; Whelan, P.; Maclennan, K. A.; Meredith, D. M.; Markham, A. F. Prostate-specific membrane antigen: evidence for the existence of a second related human gene. *Br. J. Cancer* **1995**, *72*, 583−588.

(13) Carter, R. E.; Feldman, A. R.; Coyle, J. T. Prostate-specific membrane antigen is a hydrolase with substrate and pharmacologic characteristics of a neuropeptidase. *Proc. Natl. Acad. Sci. U.S.A.* **1996**, *93*, 749−753. (b) Bzdega, T.; Turi, T.; Wroblewska, B.; She, D.; Chung, H. S.; Kim, H.; Neale, J. H. Molecular cloning of a peptidase against N−Acetylaspartylglutamate (NAAG) from a rat hippocampal cDNA library. *J. Neurochem.* **1997**, *69*, 2270−2278. (c) Luthi-Carter, R.; Berger, U. V.; Barczak, A. K.; Coyle, J. T. Isolation and expression of rat brain cDNA encoding glutamate carboxypeptidase II. *Proc. Natl. Acad. Sci. U.S.A.* **1998**, *95*, 3215−3220.

(14) Maras, B.; Greenblatt, H. M.; Shoham, G.; Spungin-Bialik, A.; Blumberg, S.; Barra, D. Aminopeptidase from *Streptomyces griseus*: primary structure and comparison with other zinc-containing aminopeptidases. *Eur. J. Biochem.* **1996**, *236*, 843−846.

(15) van Heeke, G.; Denslow, S.; Watkins, J.; Wilson, K.; Wagner, F. Cloning and nucleotide sequence of the Vibrio proteolyticus aminopeptidase gene. *Biochim. Biophys. Acta* **1992**, *1131*, 337−340.

(16) Heston, W. D. Significance of prostate-specific membrane antigen (PSMA). A neurocarboxypeptidase and membrane folate hydrolase. *Urologe A* **1996,** *35*, 400−407. (b) Rawlings, N. D.; Barrett, A. J. Structure of membrane glutamate carboxypeptidase. *Biochim. Biophys. Acta* **1997**, *1339*, 247−252. (c) Speno, H. S.; Luthi-Carter, R.; Macias, W. L.; Valentine, S. L.; Joshi, A. R. T.; Coyle, J. T. Site-directed mutagenesis of predicted active site residues in glutamate carboxypeptidase II. *Mol. Pharmacol.* **1999**, *55*, 179−185. (d) Mahadevan, D.; Saldanha, J. W. The extracellular regions of PSMA and the transferrin receptor contain an aminopeptidase domain: implications for drug design. *Protein Sci.* **1999**, *8*, 2546−2549.

(17) Minton, N. P.; Atkinson, T.; Bruton, C. J.; Sherwood, R. F. The complete nucleotide sequence of the Pseudomonas gene coding for carboxypeptidase G2. *Gene* **1984**, *31*, 31−38.

(18) Nan, F.; Bzdega, T.; Pshenichkin, S.; Wroblewski, J. T.; Wroblewska, B.; Neale, J. H.; Kozikowski, A. P. Dual function glutamate-related ligands: Discovery of a novel, potent inhibitor of glutamate carboxypeptidase II possessing mGluR3 agonist activity. *J. Med. Chem.* **2000**, *43*, 772−774. (b) Tortella, F. C.; Lin, Y.; Ved, H.; Slusher, B. S.; Dave, J. R. Neuroprotection produced by the NAALADase inhibitor 2-PMPA in rat cerebellar neurons. *Eur. J. Pharmacol.* **2000**, *402*, 31−37. (c) Kozikowski, A. P.; Nan, F.; Conti, P.; Zhang, J.; Ramadan, E.; Bzdega, T.; Wroblewska, B.; Neale, J. H.; Pshenichkin, S.; Wroblewski, J. T. Design of Remarkably Simple, Yet Potent Urea-Based Inhibitors of Glutamate Carboxypeptidase II (NAALADase). *J. Med. Chem.* **2001**, *44*, 298−301.

(19) Bairoch, A.; Apweiler, R. The SWISS-PROT protein sequence database and its supplement TrEMBL in 2000. *Nucleic Acids Res.* **2000**, *28*, 45−48.

(20) Worley, K. C.; Wiese, B. A.; Smith, R. F. BEAUTY: an enhanced BLAST-based search tool that integrates multiple biological information resources into sequence similarity search results. *Genome Res.* **1995**, *5*, 173−184.

(21) Thompson, J. D.; Higgins, D. G.; Gibson, T. J. CLUSTAL W: improving the sensitivity of progressive multiple sequence alignment through sequence weighting, positions-specific gap penalties and weight matrix choice. *Nucleic Acids Res.* **1994**, *22*, 4673−4680.

(22) Tramontano, A. Homology modeling with low sequence identity. *Methods: A Companion to Methods Enzymol.* **1998**, *14*, 293−300.

(23) Holm, L.; Sander, C. The FSSP database: fold classification based on structure-structure alignment of proteins. *Nucleic Acids Res.* **1996**, *24*, 206−210.

(24) Cuff, J. A.; Clamp, M. E.; Siddiqui, A. S.; Finlay, M.; Barton, G. J. Jpred: A Consensus Secondary Structure Prediction Server. *Bioinformatics* **1998**, *14*, 892−893. (b) Cuff, J. A.; Barton, G. J. Evaluation and Improvement of Multiple Sequence Methods for Protein Secondary Structure Prediction. *Proteins: Struct., Funct., Genet.* **1999**, *34*, 508−519. (c) Cuff, J. A.; Barton, G. J. Application of Enhanced Multiple Sequence Alignment Profiles to Improve Protein Secondary Structure Prediction. *Proteins: Struct., Funct., Genet.* **1999**, *40*, 502−511. (d) Rost, B.; Sander, C. Conservation and Prediction of Solvent Accessibility in Protein Families. *Proteins: Struct., Funct., Genet.* **1994**, *20*, 216−226.

(25) Laskowski, R. A.; Hutchinson, E. G.; Michie, A. D.; Wallace, A. C.; Jones, M. L.; Thornton, J. M. PDBsum: A Web-based database of summaries and analyses of all PDB structures. *Trends Biochem. Sci.* **1997**, *22*, 488−490. (b) Laskowski, R. A. PDBsum: summaries and analyses of PDB structures. *Nucleic Acids Res.* **2001**, *29*, 221−222.

(26) Hobohm, U.; Sander, C. Enlarged representative set of protein structures. *Protein Sci.* **1994**, *3*, 522−524. (b) Hobohm, U.; Scharf, M.; Schneider, R.; Sander, C. Selection of representative protein data sets. *Protein Sci.* **1992**, *1*, 409−417.

(27) Brooks, B. R.; Bruccoleri, R. E.; Olafson, B. D.; States, D. J.; Swaminathan, S.; Karplus, M. CHARMM: A program for macromolecular energy, minimization, and dynamics calculations. *J. Comput. Chem.* **1983**, *4*, 187−217.

(28) MacKerell, A. D.; Wiorkiewicz-Kuczera, J. J.; Karplus, M. An all-atom empirical energy function for the simulation of nucleic acids. *J. Am. Chem. Soc.* **1995**, *117*, 11946−11975. (b) MacKerell, A. D.; Bashford, J. D.; Bellott, M.; Dunbrack, R. L., Jr.; Evanseck, J. D.; Field, M. J.; Fischer, S.; Gao, J.; Guo, H.; Ha, S.; Joseph-McCarthy, D.; Kuchnir, L.; Kuczera, K.; Lau, F. T. K.; Mattos, C.; Michnick, S.; Ngo, T.; Nguyen, D. T.; Prodhom, B.; Reiher, W. E.; Roux, B.; Schlenkrich, M.; Smith, J. C.; Stote, R.; Straub, J.; Watanabe, M.; Wiorkiewicz-Kuczera, J.; Yin, D.; Karplus, M. All-atom empirical potential for molecular modeling and dynamics studies of proteins. *J. Phys. Chem.* **1998**, *102*, 3586−3616.

(29) Stote, R. H.; Karplus, M. Zinc binding in proteins and solution: a simple but accurate nonbonded representation. *Proteins* **1995**, *23*, 12−31.

(30) Jorgensen, W. L.; Chandrasekhar, J.; Madura, J. D.; Impey, R. W.; Klein, M. L. Comparison of simple potential functions for simulating liquid water. *J. Chem. Phys.* **1983**, *79*, 926−935.

(31) Rodriguez, R.; Chinea, G.; Lopez, N.; Pons, T.; Vriend, G. Homology modeling, model and software evaluation: three related resources. *Bioinformatics* **1998**, *14*, 523−528.

(32) Morris, G. M.; Goodsell, D. S.; Halliday, R. S.; Huey, R.; Hart, W. E.; Belew, R. K.; Olson, A. J. Automated Docking Using a Lamarckian Genetic Algorithm and Empirical Binding Free Energy Function. *J. Comput. Chem.* **1998**, *19*, 1639−1662.

(33) Ryckaert, J. P.; Ciccotti, G.; Berendsen, H. J. C. Numerical integration of the Cartesian equations of motion of a system with constraints: MD of *n*-alkanes. *J. Comput. Phys.* **1977**, *23*, 327−341.

(34) Steinbach, P. J.; Brooks, B. R. New spherical-cutoff methods for long-range forces in macromolecular simulation. *J. Comput. Chem.* **1994**, *15*, 667−683.
(35) Bennett, M. J.; Lebron, J. A.; Bjorkman, P. J. Crystal Structure of the Hereditary Haemochromatosis Protein Hfe Complexed with Transferrin Receptor. *Nature* **2000**, *403*, 46−53. (b) Lawrence, C. M.; Ray, S.; Babyonyshev, M.; Galluser, R.; Borhani, D.; Harrison, S. C. Crystal Structure of the Ectodomain of Human Transferrin Receptor. *Science* **1999**, *286*, 779−782.
(36) Rowsell, S.; Pauptit, R. A.; Tucker, A. D.; Melton, R. G.; Blow, D. M.; Brick, P. Crystal structure of carboxypeptidase G2, a bacterial enzyme with applications in cancer therapy. *Structure* **1997**, *15*, 337−347.
(37) Chevrier, B.; Schalk, C.; D'Orchymont, H.; Rondeau, J. M.; Moras, D.; Tarnus, C. Crystal structure of *Aeromonas* proteolytica aminopeptidase: a prototypical member of the cocatalytic zinc enzyme family. *Structure* **1994**, *2*, 283−291. (b) Chevrier, B.; D'Orchymont, H.; Schalk, C.; Tarnus, C.; Moras, D. The structure of the *Aeromonas* proteolytica aminopeptidase complexed with a hydroxamate inhibitor. Involvement in catalysis of Glu151 and two zinc ions of the cocatalytic unit. *Eur. J. Biochem.* **1996**, *237*, 393−398. (c) Greenblatt, H. M.; Almog, O.; Maras, B.; Spungin-Bialik, A.; Barra, D.; Blumberg, S.; Shoham, G. *Streptomyces griseus* aminopeptidase: X-ray crystallographic structure at 1.75 Å resolution. *J. Mol. Biol.* **1997**, *265*, 620−636.
(38) Ramachandran, G. N.; Ramakrishnan, C.; Sasisekharan, V. Stereochemistry of polypeptide chain configurations. *J. Mol. Biol.* **1963**, *7*, 95−99.
(39) Luthi-Carter, R.; Barczaka, A. K.; Spenoa, H.; Coyle, J. T. Hydrolysis of the neuropeptide *N*-acetylaspartylglutamate (NAAG) by cloned human glutamate carboxypeptidase II. *Brain Res.* **1998**, *795*, 341−349.

JM010561G